doi:10.1093/brain/awz175 BRAIN 2019: 142; 2319–2335 | 2319

BRAIN
A JOURNAL OF NEUROLOGY

TBC1D24-TLDc-related epilepsy exercise-induced dystonia: rescue by antioxidants in a disease model

Kevin Lüthy,[1,2] Davide Mei,[3] Baptiste Fischer,[4,5] Maurizio De Fusco,[6] Jef Swerts,[1,2] Jone Paesmans,[4,5] Elena Parrini,[3] Naomi Lubarr,[7] Inge A. Meijer,[8] Katherine M. Mackenzie,[9] Wang-Tso Lee,[10] Davide Cittaro,[6] Paolo Aridon,[11] Nils Schoovaerts,[1,2] Wim Versées,[4,5] Patrik Verstreken,[1,2] Giorgio Casari[12,13] and Renzo Guerrini[3,14]

Genetic mutations in *TBC1D24* have been associated with multiple phenotypes, with epilepsy being the main clinical manifestation. The TBC1D24 protein consists of the unique association of a Tre2/Bub2/Cdc16 (TBC) domain and a TBC/lysin motif domain/catalytic (TLDc) domain. More than 50 missense and loss-of-function mutations have been described and are spread over the entire protein. Through whole genome/exome sequencing we identified compound heterozygous mutations, R360H and G501R, within the TLDc domain, in an index family with a Rolandic epilepsy exercise-induced dystonia phenotype (http://omim.org/entry/608105). A 20-year long clinical follow-up revealed that epilepsy was self-limited in all three affected patients, but exercise-induced dystonia persisted into adulthood in two. Furthermore, we identified three additional sporadic paediatric patients with a remarkably similar phenotype, two of whom had compound heterozygous mutations consisting of an in-frame deletion I81_K84 and an A500V mutation, and the third carried T182M and G511R missense mutations, overall revealing that all six patients harbour a missense mutation in the subdomain of TLDc between residues 500 and 511. We solved the crystal structure of the conserved *Drosophila* TLDc domain. This allowed us to predict destabilizing effects of the G501R and G511R mutations and, to a lesser degree, of R360H and potentially A500V. Next, we characterized the functional consequences of a strong and a weak TLDc mutation (TBC1D24^{G501R} and TBC1D24^{R360H}) using *Drosophila*, where TBC1D24/Skywalker regulates synaptic vesicle trafficking. In a *Drosophila* model neuronally expressing human TBC1D24, we demonstrated that the TBC1D24^{G501R} TLDc mutation causes activity-induced locomotion and synaptic vesicle trafficking defects, while TBC1D24^{R360H} is benign. The neuronal phenotypes of the TBC1D24^{G501R} mutation are consistent with exacerbated oxidative stress sensitivity, which is rescued by treating TBC1D24^{G501R} mutant animals with antioxidants *N*-acetylcysteine amide or α-tocopherol as indicated by restored synaptic vesicle trafficking levels and sustained behavioural activity. Our data thus show that mutations in the TLDc domain of TBC1D24 cause Rolandic-type focal motor epilepsy and exercise-induced dystonia. The humanized TBC1D24^{G501R} fly model exhibits sustained activity and vesicle transport defects. We propose that the TBC1D24/Sky TLDc domain is a reactive oxygen species sensor mediating synaptic vesicle trafficking rates that, when dysfunctional, causes a movement disorder in patients and flies. The TLDc and TBC domain mutations' response to antioxidant treatment we observed in the animal model suggests a potential for combining antioxidant-based therapeutic approaches to TBC1D24-associated disorders with previously described lipid-altering strategies for TBC domain mutations.

1 VIB-KU Leuven Center for Brain and Disease Research, Leuven, Belgium
2 KU Leuven, Department of Neurosciences, Leuven Brain Institute, Leuven, Belgium
3 Pediatric Neurology, Neurogenetics and Neurobiology Unit and Laboratories, Children's Hospital A. Meyer-University of Florence, Florence, Italy
4 VIB-VUB Center for Structural Biology, Brussels, Belgium

Received December 11, 2018. Revised April 8, 2019. Accepted April 25, 2019. Advance Access publication June 29, 2019

5 Vrije Universiteit Brussel, Structural Biology Brussels, Brussels, Belgium
6 San Raffaele Scientific Institute, Milan, Italy
7 Mount Sinai Beth Israel, Department of Neurology, New York, NY, USA
8 Department of Pediatrics and Neurosciences, CHU Sainte-Justine and University of Montreal, Montreal, Canada
9 Lucile Packard Children's Hospital, Stanford University, Palo Alto, CA, USA
10 Department of Pediatrics, National Taiwan University Hospital and National Taiwan University College of Medicine, Taipei, Taiwan
11 Department of Experimental Biomedicine and Clinical Neurosciences, University of Palermo, Palermo, Italy
12 San Raffaele University, Milan, Italy
13 Telethon Institute of Genetics and Medicine, Naples, Italy
14 IRCCS Fondazione Stella Maris, Pisa, Italy

Correspondence to: Prof. Renzo Guerrini
Neuroscience Department, Anna Meyer Children's University Hospital, Florence Italy
E-mail: r.guerrini@meyer.it

Correspondence may also be addressed to: Prof. Wim Versées
VIB-VUB Center for Structural Biology, Brussels, Belgium; Vrije Universiteit Brussel,
Structural Biology Brussels, Brussels, Belgium
E-mail: Wim.Versees@vub.be

Prof. Patrik Verstreken
VIB-KU Leuven Center for Brain and Disease Research, Department of Neurosciences, Leuven, Belgium
E-mail: patrik.verstreken@kuleuven.vib.be

Prof. Giorgio Casari
San Raffaele University, Milan and Telethon Institute of Genetics and Medicine, Naples, Italy
E-mail: casari@tigem.it

Keywords: TBC1D24; Rolandic epilepsy; exercise-induced dystonia; oxidative stress

Abbreviations: NMJ = neuromuscular junction; RE-EID = Rolandic epilepsy exercise-induced dystonia; ROS = reactive oxygen species; TBC = Tre2/Bub2/Cdc16; TLDc = TBC/lysin motif domain/catalytic

Introduction

Over the last several years, more than 50 mutations in *TBC1D24* have been associated with multiple phenotypes, with drug-resistant epilepsy and DOORS syndrome being the most frequent (Balestrini *et al.*, 2016). More rare phenotypes include hearing loss, intellectual disability, cerebellar dysfunction, alternating hemiplegia and signs of neurodegeneration (Appavu *et al.*, 2016; Balestrini *et al.*, 2016; Ngoh *et al.*, 2017; Ragona *et al.*, 2017).

TBC1D24 consists of the unique association of a Tre2/Bub2/Cdc16 (TBC) and a TBC/Lysin Motif Domain/Catalytic (TLDc) domain. Missense and loss-of-function mutations are spread over the entire protein, but most affected individuals are bi-allelic mutant in the TBC domain or compound heterozygous for both the TBC and TLDc domains. Only two patients harbouring bi-allelic missense mutations in the TLDc domain have been reported, both homozygous and exhibiting as different phenotypes as DOORS syndrome (Atli *et al.*, 2018) and progressive myoclonus epilepsy (Muona *et al.*, 2015).

TBC1D24 is well conserved across species, including its *Drosophila* counterpart Skywalker (Sky). The TBC domain regulates vesicular membrane trafficking at synapses by acting with Rab-GTPases, such as Arf6 and Rab35, and docks to phosphoinositides in the membrane (Falace *et al.*, 2010; Frasa *et al.*, 2012; Fischer *et al.*, 2016). The function of the TLDc domain is less known, though a function in oxidative stress sensing or resistance has been demonstrated in cell culture (Finelli *et al.*, 2016; Finelli and Oliver, 2017). Loss of TBC1D24/Sky causes synaptic vesicle-associated proteins to excessively traffic to endosomes, where they are sorted and sent to the lysosome for degradation (Uytterhoeven *et al.*, 2011; Fernandes *et al.*, 2014). Hence, TBC1D24/Sky controls protein homeostasis at synapses, and disrupting the function of TBC1D24/Sky or pathogenic mutations in the TBC domain result in severe synaptic defects and epileptic seizures in fruit flies (Fischer *et al.*, 2016) as well as neuronal architectural defects in rodent neurons (Falace *et al.*, 2010, 2014; Milh *et al.*, 2013). *In vivo* experiments in rodents confirm that genetic disruption of Tbc1d24 impairs vesicle trafficking and spontaneous neurotransmission, resulting in seizures and early death (Finelli *et al.*, 2019; Tona *et al.*, 2019).

Here we demonstrate that the three affected individuals of the original Rolandic epilepsy (RE)-writer's cramp-exercise induced dystonia (EID) pedigree (Guerrini *et al.*, 1999) (http://omim.org/entry/608105) harbour compound heterozygous missense mutations in the TBC1D24 TLDc domain. Through a two-decade follow-up we observed that while epilepsy had a self-limited course, EID persisted into

adulthood in two of the three patients, though with reduced severity. Furthermore, we identified three sporadic patients of paediatric age with a remarkably similar RE-EID phenotype who harboured bi-allelic TBC1D24 mutations, each including an amino acid substitution in close proximity in the TLDc domain. By solving the crystal structure of the TLDc domain we show how the mutations could destabilize and/or affect its fold. Using *Drosophila* as a model, we found that the TLDc domain mediates reactive oxygen species (ROS)-induced defects in synaptic vesicle trafficking. Indeed, TLDc pathogenic mutations cause a molecular phenotype comparable to that of high ROS load. Both cellular and behavioural defects of mutant animals are rescued by antioxidant feeding. We propose here that the TBC1D24/Sky TLDc domain is a direct or indirect ROS sensor mediating synaptic vesicle trafficking rates that, when dysfunctional, causes a movement disorder in patients and flies.

Materials and methods

Patients

Original RE-EID pedigree

A brother, sister and their first cousin were products of consanguineous marriages between two brothers and two sisters (Patients 1-VII:2, 2-VII:3 and 3-VII:4) (Fig. 1A) of Italian ancestry. They exhibited a syndrome with onset in infancy, featuring focal seizures, often hemifacial, centro-temporal EEG abnormalities, and paroxysmal dystonia precipitated by sustained exercise (Guerrini *et al.*, 1999). They also exhibited forearm dystonia that caused writing to progressively become scribbling and then made it impossible after a few minutes. This manifestation is more akin to EID involving forearm muscles than to classical writer's cramp in which dystonic posturing appears as soon as writing starts. These three patients, aged 11, 22 and 23 years at the time of our original description (Guerrini *et al.*, 1999) have been under clinical follow-up for 20 further years.

Patients 4–6

These three sporadic patients were identified as exhibiting a phenotype similar to the original RE-EID family during an international paediatric movement disorders workshop in Barcelona, Spain, in February 2019. Clinical histories, video-recordings of seizures and EID attacks and next generation sequencing data were shared and reviewed. Patients 4 and 5 were studied in the USA and were of Italian and Han Chinese ancestry, respectively; Patient 6 was studied in Taiwan and was of Han Chinese ancestry.

WES and WGS analysis

All participants had signed an informed consent for research or diagnostic whole exome/genome sequencing (WES/WGS) in the participating institutions. Consent was obtained according to the Declaration of Helsinki. Written consent was also obtained for the video recordings shown in the Supplementary material. The study was approved by the Paediatric Ethic Committee of the Tuscany Region in the context of the DESIRE project (EC, Seventh Framework Programme, grant agreement 602531). Methods used for WES and WGS are reported in detail in the Supplementary material.

Bioinformatic impact predictions

We evaluated mutations' pathogenicity of *TBC1D24* variants through *in silico* prediction using the dbNSFP database (v3.3a) (Liu *et al.*, 2016) and the scores obtained from Revel (Ioannidis *et al.*, 2016), M-CAP (Jagadeesh *et al.*, 2016) and Eigen (Ionita-Laza *et al.*, 2016), three different tools to evaluate the pathogenicity of rare variants.

To improve the information obtained by the variant-level CADD, PolyPhen-2 and SIFT impact predictions, we also used the mutation significance cutoff (MSC) server (http://pec630.rockefeller.edu:8080/MSC/), a quantitative approach that provides gene-level and gene-specific phenotypic impact cut-off values.

Finally, a multiple sequence alignment of the *TBC1D24* orthologous protein sequences was generated by the Jalview software (http://www.jalview.org) with colour-coding for physicochemical properties (Zappo colour scheme).

Drosophila stocks and genetics

Fly stocks were maintained on standard medium at 21°C and a 12-h light/dark cycle. Larvae or adult animals were selected for the correct genotype and age-matched flies of other conditions and genotypes were selected for testing. After assigning letters to each experimental group, the order of testing was randomized. Neuronal human TBC1D24 was expressed in *sky* mutation background (Uytterhoeven *et al.*, 2011). The ROS scavengers, antioxidants *N*-acetylcysteine amide (AD4, 40 µg/ml) (Jung *et al.*, 2017) or α-tocopherol (vitamin E, 20 µg/ml) (Driver and Georgeou, 2003), were added to the food source and refreshed in adult food source 48 h prior to testing. To optimize solubility, α-tocopherol (vitamin E) was dissolved in water and 0.0005 final volume per cent ethanol in two consecutive steps. AD4 was dissolved in pure water. For controls, solvent (H_2O) without antioxidants was added. Transgenic flies were generated (Fischer *et al.*, 2016) from gBlocks (IDT) of the human coding sequences (Supplementary Table 1). pUAST.attB-GFP::TBC1D24^{WT} under a 5xUAS-hsp70 promoter and three pathogenic alleles were generated by site-directed mutagenesis: G501R and R360H as well as TBC domain mutation R40C (Supplementary Table 2) and verified by sequencing analysis. For the ΔTLDc construct, pUAST.attB-GFP::TBC1D24^{WT} was digested with KpnI-EcoRI, resulting in the deletion of the cDNA of TBC1D24. TBC1D24 without the TLDc domain was synthesized by performing a PCR reaction on this plasmid with primers FW TBC1D24-ΔTLDc (GCTGTACAAAGGTGGGGGT) and RC TBC1D24-ΔTLDc (TTCACAAAGATCCTAAGCTTGAATTCTACAACGCTTTTT-CGTTGG). This PCR fragment was introduced in the digested vector by Gibson Assembly. The resulting plasmid pUAST.attB-GFP::TBC1D24$^{\Delta TLDc}$ was confirmed by sequencing. For crystal structure analysis, the DNA sequence coding for the TLDc domain of Skywalker (residues 401–587) was amplified from *Drosophila sky* (CG9339, isoform A), inserted into plasmid pet28-Sky401–587 and sequencing verified plasmid transformed into *E. coli* C41(DE3) (Novagen).

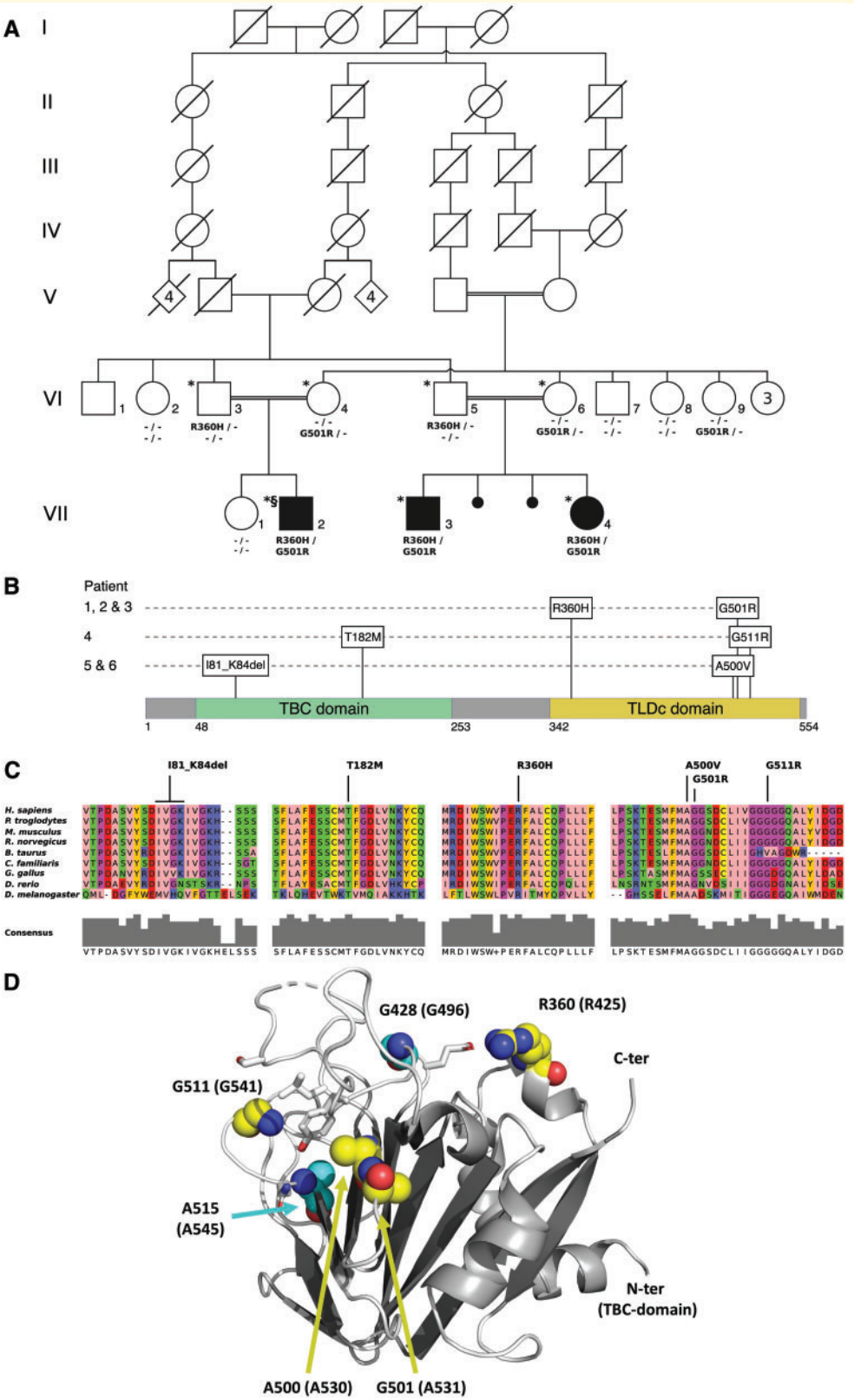

Figure 1 Patients and mutations. (**A**) Original RE-EID pedigree. Sequencing identified a novel pathogenic human TBC1D24 TLDc domain compound heterozygous variant, TBC1D24G^{501R} / TBC1D24R^{360H} in three patients in the same generation. The phenotype of epilepsy and paroxysmal EID (with writer's cramp) was autosomal recessive for all patients. *Whole exome sequencing performed; *§Whole exome and genome sequencing performed. (**B**) TBC1D24 domain organization depicting the location of the mutations identified in the original RE-EID pedigree (Patients 1-VII:2, 2-VII:3 and 3-VII:4) and in the additional unrelated patients with the same phenotype (Patients 4–6). (**C**) Multiple sequence alignment between human TBC1D24 and orthologous sequences. Residues were coloured according to their physicochemical

(continued)

Behaviour assays

Single-blinded behaviour experiments were performed on third-instar larvae and adults. Animals were optically screened for correctly folded wings and healthy walking behaviour. Male adults 2–5 days after enclosure were tested by flight and seizure assays (Fischer *et al.*, 2016), with seizure assays starting set to two 1-min steps, with 1-min rest. Activity scores for paralysed, slowed and unaffected flies were measured and testing repeated after 5 min.

Negative geotaxis assays measured five repetitions of sustained climbing activity (Benzer, 1967) in 30-s steps, repeated after 5 min. Larval light-avoidance determined coordinated movement (Sawin-McCormack *et al.*, 1995).

Protein expression and purification

The DNA sequence coding for the TLDc domain of Skywalker (residues 401–587) was amplified from the *Drosophila sky* gene (CG9339, isoform A), and cloned into the pet28 plasmid (Novagen). Expression and purification of the His-tagged TLDc domain, using a HisTrap column and size-exclusion chromatography, were performed as previously described for the Sky TBC domain (Fischer *et al.*, 2016). Prior to the gel filtration step, the 6xHis tag was removed by overnight incubation with 1% mg/mg thrombin protease followed by a second passage over a HisTrap column to remove uncleaved protein. The protein was concentrated to 10 mg/ml in a buffer containing 25 mM HEPES pH 7.5, 150 mM NaCl and 10% glycerol, flash-frozen in liquid nitrogen and stored at −80°C.

Crystallization and structure determination

Crystals of the $Sky_{401–587}$ protein were obtained at 4°C in 28% PEG 3350, 0.1 M HEPES pH 7.5 and 0.6 M ammonium citrate. Prior to freezing in liquid nitrogen, the crystals were transferred to cryoprotectant solution consisting of the mother liquor with 20% glycerol.

The $Sky_{401–587}$ crystals diffracted to 2.05 Å resolution. A complete dataset was collected at 100 K on the Proxima 2 beamline (SOLEIL synchrotron). Data processing and scaling was carried out using XDS and XSCALE (Kabsch, 2010). The structure was solved by molecular replacement using the zebrafish Oxr1 structure as a model (pdb 4ACJ) with Phaser (McCoy *et al.*, 2007). The model was then improved by iterative cycles of refinement with Phenix and manual building in Coot (Emsley *et al.*, 2010). MolProbity was used for structure validation (Chen *et al.*, 2007). X-ray data collection and refinement statistics are listed in Supplementary Table 3. All structural figures were produced with PyMOL (http://www.pymol.org/).

Protein folding free energy prediction

Calculation of the folding stability was performed using PoPMuSiC-2.0 (Dehouck *et al.*, 2009) and Site Directed Mutator (SDM) (Worth *et al.*, 2011).

Imaging

FM1–43 dye uptake

Neuromuscular FM1–43 (4 µM) (Invitrogen) dye uptake at larval muscle 6/7 NMJs (neuromuscular junctions) was carried out as previously described (Fischer *et al.*, 2016) to quantify FM1–43 foci from 0.4 µm optical slices in single-blinded analysis.

Transmission electron microscopy

Third-instar larval NMJs were prepared for transmission electron microscopy (TEM) and imaged as described previously (Fischer *et al.*, 2016). To analyse double-blinded synaptic bouton data, ultrastructural profile areas and synaptic-vesicle content were quantified in ImageJ as previously described (Fischer *et al.*, 2016).

In vivo fluorescence imaging

Third-instar larvae expressing GFP-tagged TBC1D24 were dissected in HL-3 on Sylgard plates, and the NMJs of third-instar larvae were recorded by live imaging with a Nikon A1R confocal microscope and a ×60, 1.0-NA water immersion lens in stacks of 0.5 µm optical sections with standard GFP optics. Images are the maximum intensity projections of three consecutive slices through the NMJ.

Peroxide stimulation

To induce oxidative stress at the *Drosophila* larval NMJ, we incubated dissected larvae in HL-3 physiological solution containing 50 mM H_2O_2 for 15 min (Slabbaert *et al.*, 2016). Before nerve cell stimulation, animals were washed with HL-3 and nerve cords were cut prior to application of 90- or 60-mM stimulation solution for FM1–43 labelling or for TEM, respectively.

Statistical analysis

Gaussian distribution per genotype and condition was determined with D'Agostino-Pearson normality tests, following respective Welch's or Mann-Whitney *t*-tests. Multiple comparisons with

Figure 1 Continued

properties (Zappo colour scheme). Residues affected by the identified mutations are indicated. (**D**) X-ray crystal structure of the TLDc domain of the fly TBC1D24 orthologue (Sky) and mapping of the residues affected by pathological mutations. The structure of the TLDc domain (residues 403 to 587) of the fly TBC1D24 orthologue is shown in cartoon representation, with β-strands, α-helices and loops coloured in different shades of grey. A flexible loop region (residues 517 to 520) that could not be modelled in the structure is indicated by a dotted curved line. Residues affected by mutations in patients identified in this study are shown in sphere representation with carbon atoms coloured yellow. Residues corresponding to patient mutations that have been reported previously, but are discussed in this paper, are shown as spheres with carbon atoms coloured cyan. Close-up views of the region surrounding these affected residues are shown in Supplementary Fig. 2.

one-way ANOVA utilized Dunnett's or Kruskal-Wallis tests based on the outcome of normality tests. H_2O_2 stimulation effects were determined by two-way ANOVA for significant effects of either genotype, peroxide stimulation or both conditions. Box plots are described in the figure legends; bar graph error bars represent the standard error of the mean (SEM).

Data availability

The authors confirm that the data supporting the findings of this study are available within the article and/or its Supplementary material. Raw sequencing data of this study are available from the corresponding author on request. Structure coordinates and structure factors have been deposited in the PDB with accession code 6R82.

Results

Mutations in the TBC1D24 TLDc domain cause RE-EID

Patients 1-VII:2, 2-VII:3 and 3-VII:4, first described in the initial report of familial RE-EID are now aged 31, 42 and 43 (Table 1). Focal motor seizures, which manifested infrequently since infancy, never relapsed under carbamazepine or oxcarbazepine treatment after ages 16, 18 and 22 (Supplementary Video 1). Exercise-induced dystonia (Supplementary Videos 2 and 3) was instead still present at last follow-up in two patients, although attacks became much less frequent in adulthood, with both patients reporting to have learned how to limit fatigue or physical exercise by modulating their activities. All three patients still exhibited mild nystagmus and postural tremor of the hands and were treated with trihexyphenidyl as an anti-tremor drug. Treatment with carbidopa/L-DOPA and acetazolamide failed to prevent dystonic attacks. Treatment with ubidecarenone was tentatively started at 30 years of age in Patient 3-VII:4 who reported no sizeable overall benefits and ceased medication after 2 months, as seizures had long been under remission and attacks of EID were rare at the time. Brain MRI, repeated in adulthood, has remained normal in all three patients.

In our original description, we linked the disease locus to a large homozygous region on chromosome 16 (Guerrini *et al.*, 1999). Sequencing of the critical region (mean depth of 136) for identifying the causative gene under a recessive consanguineous model (multiple loops of consanguinity are present in the pedigree) and, therefore, looking for a consistent homozygous mutation common to the three individuals, failed (Supplementary Table 4). We finally extended the analysis to a recessive model including compound heterozygous mutations.

Only two genes, *ZNF717* and *TBC1D24*, qualified for the compound heterozygous model (Supplementary Table 5). As the *ZNF717* gene is prone to misinterpretation of pathogenicity (Kwak *et al.*, 2017), the *TBC1D24* gene remained the only candidate, displaying both mutations within the

Table 1 Summary of clinical features in the RE-EID patients

	Patient 1-VII:2 Male c.[1079G>A];[1501G>A] p.[R360H];[G501R]	Patient 2-VII:3 Male c.[1079G>A];[1501G>A] p.[R360H];[G501R]	Patient 3-VII:4 Female c.[1079G>A];[1501G>A] p.[R360H];[G501R]	Patient 4 Female c.[545C>T];[1531G>A] p.[T182M];[G511R]	Patient 5 Female c.[241_252del];[1499C>T] p.[I81_K84del];[A500V]	Patient 6 Male c.[241_252del]; [1499C>T] p.[I81_K84del];[A500V]
Age at seizure onset / outset	1 year / 22 years	4 years / 16 years	3 years / 22 years	1 year / 13 years (still present)	11 months / 8 years (still present)	6 months / 9 years
Seizure type	Focal motor, generalized tonic-clonic	Focal motor	Focal motor	Focal motor	Focal motor	Focal motor
Age at onset of exercise induced dystonia	3 years	4 years	2 years	3 years	4 years	2 years
Age at follow-up / last brain MRI scan in adulthood	43 years / normal	42 years / normal	31 years / normal	13 years / normal	8 years / normal	12 years / normal
Long-term EID outcome	Last attack at 8 years	Still present, rare	Still present, rare	Last attack at 8 years	Still present	Still present
Additional manifestations	Nystagmus, postural hand tremor	Nystagmus, postural hand tremor	Nystagmus, postural hand tremor	Postural hand tremor	None	Postural hand tremor

TLDc domain (accession NM_001199107.1), c.1079G>A (p.R360H) and c.1501G>A (p.G501R) (Fig. 1B and Supplementary Fig. 1). The c.1501G>A variant was not reported in the Genome Aggregation Database (gnomAD - https://gnomad.broadinstitute.org/) whereas the c.1079G>A variant was reported in gnomAD with a low frequency (4/267 568 alleles) (Supplementary Table 6A). The two missense substitutions involved evolutionarily conserved residues in orthologues (Fig. 1C) and were predicted to be damaging by MSC CADD, PolyPhen-2 and SIFT corrected scores (Supplementary Table 6B).

Patient 4 is a 13-year-old female. In the first year of life, lateralized clonic jerks of the hand and face were first noticed. These episodes, which have the semiology of Rolandic seizures (Supplementary Video 4) still occur occasionally, lasting a few minutes. At age 2 years, she developed episodes of dysarthria and swallowing difficulties, which would last for hours and resolve with sleep. Interictal EEGs were normal but these episodes were never recorded. Starting in early childhood, she experienced episodes of paroxysmal truncal dystonia with arching of the back and involuntary movements, which would last seconds to minutes, often prompted by fatigue or excitement (Supplementary Video 5). All episodes were more frequent when she was sleep deprived. With oxcarbazepine and carbidopa/levodopa treatment and using clonazepam prophylactically when exposed to a known trigger, episodes of dystonia have not recurred in the last 3 years. However, she has a tight right-hand grip while writing (Supplementary Video 6) and bilateral arm tremor when performing fine motor tasks. She had exertional components also related to speech and voice, with shaking of jaw and tongue by chewing harder foods or stuttering triggered by talking or singing for longer periods. Her neurological function is otherwise normal and brain MRI is unremarkable. WES identified two heterozygous mutations in the *TBC1D24* gene: c.545C>T (p.T182M) (paternally inherited) and c.1531G>A (p.G511R) (maternally inherited) (Fig. 1B and Supplementary Fig. 1). The c.545C>T variant was reported in gnomAD with a low frequency (1/248 856 alleles) whereas the c.1531G>A variant was not reported in gnomAD (Supplementary Table 6A). The two novel missense substitutions involved evolutionarily conserved residues in orthologues (Fig. 1C) and were predicted to be damaging by MSC CADD, PolyPhen-2 and SIFT corrected scores (Supplementary Table 6B).

Patient 5 is an 8-year-old female who first manifested brief jerking episodes that were exacerbated by fever and interpreted as myoclonic jerks at 11 months. These manifestations subsequently intensified and clearly involved the face, causing drooling and dysarthria, or the hand, on either side, consistently with Rolandic-type focal motor seizures (Supplementary Video 7). At around age 4, EID also appeared with prominent truncal arching (Supplementary Video 8) and inability to stand, lasting several minutes. Levetiracetam, oxcarbazepine and valproic acid provided no benefit to clinical manifestations, which were, however, less frequent and shorter under benzodiazepine treatment. Brain MRI was normal. Interictal EEG showed left temporal sharp waves. Neurological examination was normal. WES identified two heterozygous mutations in the *TBC1D24* gene: c.241_252delATCGTGGGCAAG (p.I81_K84del) (maternally inherited) and c.1499C>T (p.A500V) (paternally inherited) (Fig. 1B and Supplementary Fig. 1).

Patient 6 is a 12-year-old male who exhibited episodes of involuntary movements and weakness since infancy. These episodes could affect either side and last from several minutes to hours but it became apparent over time that they occurred after prolonged exercise and that resting would reduce their duration. They were not improved by flunarizine or acetazolamide. Tremor of the hands was also noticed. When the boy was 6 months old, focal motor seizures also appeared, which remained rare but could at times be prolonged up to 20 min. Treatment with lacosamide and clobazam had limited effect, and lamotrigine was beneficial. His last seizure occurred when he was aged 9, but episodes of EID are still present. Brain MRI was normal. EEG showed diffuse and focal discharges over both fronto-central areas. WES identified compound heterozygous mutations identical to Patient 5 (I81_K84del and A500V) (Fig. 1B and Supplementary Fig. 1).

The Han Chinese ancestry common to Patients 5 and 6 might suggest a founder effect. Both mutations are present in databases, where the TLDc mutation A500V is very rare. In contrast, the in-frame deletion I81_K84del within the TBC domain is quite frequent among East Asian individuals, reaching a frequency of 1.2×10^{-3} (Supplementary Table 6A).

The two mutations identified in Patients 5 and 6 involve evolutionarily conserved residues in orthologues (Fig. 1C) and the A500V missense substitution is predicted to be damaging by MSC CADD, PolyPhen-2 and SIFT corrected scores (Supplementary Table 6B). The I81_K84del in-frame deletion has been identified, as homozygous variant, in a patient with epilepsia partialis continua and generalized tonic-clonic seizures (Zhou *et al.*, 2018). The A500V missense substitution had been identified twice previously. In a first report it occurred *in trans* with the F229S missense substitution, in a 2-year-old male whose clinical characteristics are succinctly described as episodes of 'myoclonic jerking of the face and arms' (Balestrini *et al.*, 2016). In the second report it occurred *in trans* with the S473Rfs*43 frameshift mutation, in a 4-year-old female who had manifested 'rhythmic unilateral facial spasms' in the first year of life, cerebellar ataxia and episodes 'non-convulsive status epilepticus' (Li *et al.*, 2018). While for both patients the above descriptions appear to include focal motor seizures involving the face, as observed in our patients, their young age precludes knowledge of whether they also developed EID.

Among the >50 patients carrying bi-allelic *TBC1D24* mutations reported to date (Balestrini *et al.*, 2016), only two have homozygous missense mutations in the TLDc domain (Muona *et al.*, 2015; Atli *et al.*, 2018). One patient, homozygous for p.R360L, exhibited progressive myoclonus epilepsy (Muona *et al.*, 2015). The other patient,

homozygous for p.G428R, exhibited DOORS syndrome (Atli *et al.*, 2018). There are no previous reports of patients harbouring compound heterozygous missense substitutions both residing within the TLDc domain. All the RE-EID patients reported here harbour bi-allelic TBC1D24 mutations that can be described as hypomorphic TBC mutations (or mildly affecting the protein function as the R360H) coupled to severe TLDc missense mutations clustering within 500 to 511 residues, which seems to be the hallmark for this condition. Among all TBC1D24 missense mutations reported previously, only A515V is located in the proximity of these residues. Functional experiments suggest that the A515V mutation, observed *in trans* with the D147H mutation in a family with infantile myoclonic epilepsy, impaired neurite growth and length compared to wild-type TBC1D24 (Falace *et al.*, 2010) but did not influence neuroprotective properties to oxidative stress response assays (Finelli *et al.*, 2016).

The TLDc crystal structure predicts an effect of mutations on protein stability and/or conformation

To understand how the mutations we identified in patients with epilepsy and EID might affect TLDc domain integrity and functionality, we solved the X-ray crystal structure. While we have not been able to crystallize the human TLDc domain, this domain is well conserved across species and the *Drosophila* Sky TLDc domain ($Sky_{401–587}$) was crystallized. $Sky_{401–587}$ crystallizes in the $P4_32_12$ space group with two (monomeric) protein molecules in the asymmetric unit and crystals diffracted to 2.05 Å. The structure was solved by molecular replacement using Oxr1 from zebrafish as a model (pdb 4ACJ) (Blaise *et al.*, 2012). Clear electron density is present for most of the peptide chain except for the residues 401–402 and 517–520 from monomer A, and residues 401–412, 485–489 and 517–519 from monomer B (using the *Drosophila* Sky residue numbering), which are not modelled. The overall fold of $Sky_{401–587}$ is similar to Oxr1 with the protein adopting an $\alpha + \beta$ fold constituted of 11 β-strands organized in a six-stranded and a five-stranded anti-parallel β-sheet that are stacked together, and five surrounding short α-helices (Fig. 1D). However, $Sky_{401–587}$ contains two long and flexible loops with additional amino acids (residues 474–498 and 511–528) when compared to Oxr1.

Next, we mapped the pathogenic mutations on the TLDc structure. The residues G501, G511 and A500 that are found mutated in Patients 1–3, Patient 4 and Patients 5 and 6, respectively, are located on the same side of the protein and correspond to A531, G541 and A530 in *Drosophila* Sky (Fig. 1D). An A515V mutation that was previously identified in a family with infantile myoclonic epilepsy (see above, Falace *et al.*, 2010) also locates to the same site, with A515 corresponding to A545 in Sky. The $Sky_{401–587}$ crystal structure shows that G501/A531 is buried in the protein (Supplementary Fig. 2), and a G501R/A531R mutation would cause very severe steric clashes and thus a loss of protein domain stability. This is supported by *in silico* calculation of the thermal stability of the G501R/A531R mutant, using two different predictors (PopMusic-2.0 and SDM) (Table 2). While amino acid residue G511/G541 is rather solvent exposed, its mutation to an arginine residue could cause steric clashes with the surrounding T494/S524 and M497/L527 residues (Fig. 1D and Supplementary Fig. 2). Moreover, G511/G541 is part of a conserved glycine-rich region at the tip of a loop region connecting two β-strands. Mutating one of these glycines to a conformationally more restrained arginine residue could destabilize this loop or affect its functionality. In agreement, both PopMusic-2.0 and SDM predict a strong destabilizing effect of the G511R/G541R mutation (Table 2). In contrast to G501/A531, which points toward the interior of the protein, A500/A530 points with its side chain toward the outside of the protein. Consequently, the stability predictors do not predict an effect of the corresponding A500V/A530V mutation on overall protein stability (Table 2). Nevertheless, closer inspection of the structure shows that a A500V/A530V mutation would lead to a steric clash of the valine side chain with the side chain of F424/Y492 (Supplementary Fig. 2). Movement of the F424/Y492 side chain to accommodate the A500V/A530V mutation could in turn affect the conformation and function of the loop containing both G511/G541 and A515/A545. In turn, A515/A545 is pointing toward the interior of the protein, and based on the structure, a A515V/A545V mutation is expected to lead to steric strain and destabilization (Supplementary Fig. 2). Nevertheless, only one of the two predictors (SDM) predicts a destabilization caused by the A515V/A545V mutation (Table 2). The R360/R425 and G428/G496 residues are located on the opposite side of the structure in comparison to the previously discussed residues (Fig. 1D) and are indirectly connected via a salt bridge between the side chains of R360/R425 and E429/E497, just adjacent to G428/G496 (Supplementary Fig. 2). An R360H/R425H or R360L/R425L mutation would disrupt this salt bridge. These mutations are predicted to only cause a mild effect on protein stability but could change the conformation of the involved peptide loops. Correspondingly, also a G428R/G496R mutation could change the conformation of these loops, and, moreover, introduction of the bulky arginine side chain could cause a destabilization of the local fold by steric hindrance with respect to the adjacent and conserved W444/W512 residue (Supplementary Fig. 2).

TBC1D24 TLDc domain mutations do not affect protein localization in neurons

We continued further studies with a strongly and a weakly destabilizing TLDc domain point mutation, located at

Table 2 Prediction of the effect of the clinical mutations on the stability of the Sky TLDc domain

Mutation TBC1D24/ Skywalker	Patient	Prediction method (ΔG in kcal/mol)	
		PopMusic-2.0	SDM
R360H / R425H	1, 2 and 3	−0.2	−0.6
R360L / R425L	Muona *et al.*, 2015	0.0	0.0
G428R / G496R	Atli *et al.*, 2018	−1.0	−1.5
A500V / A530V	5 and 6	+0.2	+0.9
G501R / A531R	1, 2 and 3	−0.9	−2.1
G511R / G541R	4	−1.5	−4.1
A515V / A545V	Falace *et al.*, 2010	+0.2	−0.7

−ΔG: Negative values of ΔG indicate a destabilization; the larger the destabilizing effect the more negative the ΔG value.
SDM = site direct mutagenesis.

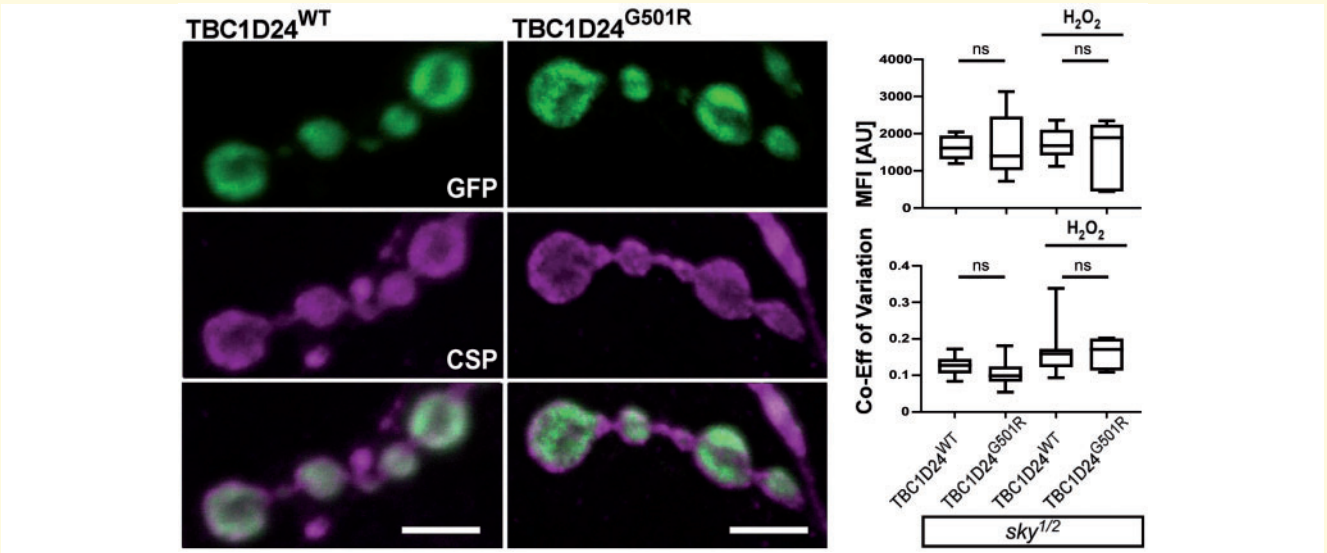

Figure 2 Human GFP::TBC1D24 protein distribution following expression at the *Drosophila* NMJ. Expression levels (*top* graph) and synaptic distribution (*bottom* graph) of the GFP::TBC1D24 fusion protein compared to antibody-labelled CSP at third-instar NMJs of TBC1D24^{WT} and TBC1D24^{G501R} animals indicates that TBC1D24, like Skywalker, is localized predominantly in the periphery of synaptic boutons. Scale bar = 5 μm. One-way ANOVA: ns = not significant $P > 0.05$.

opposite sides of the structure: G501R and R360H, respectively. To start testing the functional effects *in vivo*, we generated fruit flies expressing wild-type and mutant GFP-tagged human TBC1D24 instead of the endogenous fly homologue Sky (Uytterhoeven *et al.*, 2011). *Sky* mutants die during development, but mutants expressing wild-type human TBD1C24 in their neurons (nSyb-Gal4) survive. Similarly, *sky* mutants that express pathogenic mutant GFP-tagged TBC1D24 also live, albeit with behavioural defects (see below). These data indicate that human TBC1D24 is functional in flies and can compensate for the loss of fly *sky*.

GFP-TBC1D24 expressed in neurons of *sky* mutants is transported to synaptic terminals and localizes to presynaptic boutons of the NMJ; very little TBC1D24 localizes to the inter-bouton regions or axons, likewise to wild-type *Drosophila* Sky (Uytterhoeven *et al.*, 2011) (Fig. 2). Similarly, pathogenic mutant TBC1D24^{G501R} or TBC1D24^{R360H} concentrate at presynaptic boutons (Fig. 2 and not shown). These data indicate that human TBC1D24 expressed in neurons preferentially localizes to synaptic regions, resembling endogenous wild-type fly Sky, and that the pathogenic G501R and R360H in TBC1D24 do not noticeably affect protein abundance or localization.

TLDc domain mutations induce sustained-activity locomotion defects

Reported mutations in the TBC domain of TBC1D24 or Sky cause seizures in patients (Balestrini *et al.*, 2016) and in fruit flies (Fischer *et al.*, 2016). To determine if the TLDc mutations we selected for experimental purposes cause seizure-like behaviour in fruit flies, we performed seizure assays with the respective genotypes. While *sky* mutants that

express TBC1D24 with mutations in the TBC domain (e.g. TBC1D24^{R40C}) (Fig. 3A) show severe and long-lasting seizure-like activity (Fischer *et al.*, 2016) (Fig. 3B), *sky* mutants that express TLDc domain mutations TBC1D24^{G501R} or TBC1D24^{R360H} (Fig. 3A) do not and they are very similar to *sky* mutants that express wild-type human TBC1D24 (Fig. 3B). We quantified the activity of TBC and TLDc mutant flies by calculating an activity score based on the time it takes the flies to recover after the vortex stimulation, in comparison to controls expressing TBC1D24^{WT}. These data indicate that pathogenic mutations in the TLDc domain do not result in obvious seizure-like activity in fruit flies.

Next, we assessed other locomotion-based behaviour. We tested sustained activity by assessing if flies sustain climbing activity (negative geotaxis) over the course of five-step trials. We found that *sky* mutants that express TBC1D24^{G501R} display a significantly lower activity score compared to controls (*sky* mutants that express TBC1D24^{WT}; Fig. 3C). *Sky* mutants that express TBC1D24^{R40C} do not show a defect in this assay, while TBC1D24^{R360H} display even more activity.

We also tested coordinated movements based on larval light-avoidance and determined whether *sky* mutant larvae that express wild-type or mutant TBC1D24 are able to sense and leave bright areas. We found that the preference indices (PI) to move to a non-lit area of animals expressing TBC1D24^{G501R} are significantly lower than those of controls but also of those of animals expressing TBC (TBC1D24^{R40C}) or weak TLDc (TBC1D24^{R360H}) mutants (Fig. 3D). Hence, the data are consistent with TBC1D24^{G501R} being a more severe mutation than TBC1D24^{R360H} and they also indicate the TBC1D24^{G501R} mutation causes a distinct phenotype from the TBC domain mutation including sustained and coordinated movement defects.

Synaptic trafficking defects in TBC1D24-TLDc mutants

Sky/TBC1D24 acts via Rab35-dependent synaptic vesicle transport (Uytterhoeven *et al.*, 2011; Falace *et al.*, 2014; Sheehan and Waites, 2019) and controls protein homeostasis, as *sky* loss promotes protein trafficking to recycling endosomes where these synaptic vesicle proteins are sorted for degradation (Uytterhoeven *et al.*, 2011). To assess synaptic vesicle trafficking efficiency in *sky* mutant animals expressing TLDc domain mutations, we used FM1–43. FM1–43 is a lipophilic dye that upon nerve stimulation is internalized in newly formed synaptic vesicles and allows us to follow the fate of newly endocytosed vesicles at synaptic terminals (Ramaswami *et al.*, 1994). In controls, FM1–43 uniformly labels the synaptic vesicle pool that organizes in a typical doughnut-like shape (Estes *et al.*, 1996) (Fig. 4A), but in severe hypomorphic *sky*$^{1/2}$ or *sky*$^{2/d0}$ mutants FM1–43 frequently concentrates in puncta (Fig. 4A, middle and B, arrowheads) that we demonstrated previously to have endosome identity (Uytterhoeven *et al.*, 2011). Similarly, we found FM1–43 puncta in *sky*

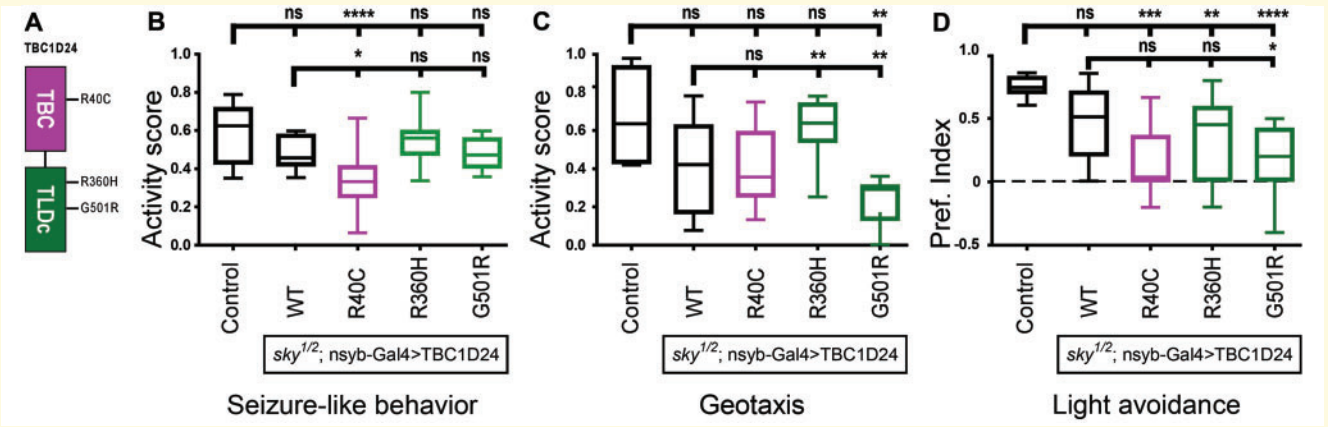

Figure 3 Behaviour. Patient mutations cause activity-related defects in adult and larval Drosophila model. (**A**) Colour-coded schematic of the TBC and TLDc domain mutations in TBC1D24 protein. (**B**) Neuronal overexpression of the human TBC1D24^{R360H} or TBC1D24^{G501R} mutations on *sky*$^{1/2}$ deficiency background. Adult fly seizure-like behaviour assays indicated no difference in the activity scores of either mutation in comparison to wild-type w^{1118} and to wild-type TBC1D24 controls. (**C**) In contrast, sustained activity of TBC1D24^{G501R} animals is significantly impaired compared to TBC1D24^{WT}. *n* = 30–60 animals in two technical replicates (negative geotaxis), one-way ANOVA TBC1D24^{WT} versus TBC1D24^{R40C}, TBC1D24^{R360H}, TBC1D24^{G501R}: **P* = 0.032, ns = not significant. TBC1D24^{G501R} third-instar larvae exhibit deficits in coordinated movement. (**D**) In TBC1D24^{G501R} animals, the light-avoidance reaction is absent in comparison to TBC1D24^{WT} and TBC1D24^{R360H}. Adult assays, tested in two technical replicates per group of 10 animals. Graphs show box-and-whisker plots defined by a bar for the median. Interquartile intervals are visualized as boxes and minimum/maximum as whiskers. Dunnett's test (seizure-like behaviour): TBC1D24^{WT} versus TBC1D24^{R40C}, TBC1D24^{R360H}, TBC1D24^{G501R}: **P* = 0.0124, ns = not significant P = 0.2476, ns = not significant *P* > 0.9999. *n* = 30–80 animals. Holm-Sidak's test (negative geotaxis): TBC1D24^{WT} versus TBC1D24^{R40C}, TBC1D24^{R360H}, TBC1D24^{G501R}: ns = not significant *P* = 0.9732, ***P* = 0.0076, ***P* = 0.0088. *n* = 30–60 animals. Larval assays, tested in two technical replicates per group of 10 animals: Dunnett's test: TBC1D24^{WT} versus TBC1D24^{R40C}, TBC1D24^{R360H}, TBC1D24^{G501R}: ns = not significant *P* = 0.0575, ns = not significant *P* = 0.5029, **P* = 0.029. *n* = 30–40 animals.

mutants that express TBC1D24^{G501R} (Fig. 4A and C). Note, however, that this phenotype is much milder than in the strong hypomorphic *sky* mutants, but similar to the phenotype we observed previously in *sky* mutant animals that express the pathogenic TBC domain mutation (TBC1D24^{R40C}) (Fig. 4C) (Fischer *et al.*, 2016). Only a non-significant trend towards an increase in puncta density was measured in the weak TLDc mutation TBC1D24^{R360H}. Finally, the total amount of FM1–43 dye uptake was also not affected by the mutants (Fig. 4E). This indicates that mutations in the TBC and TLDc domain affect synaptic membrane trafficking but not the uptake of membrane by endocytosis *per se*.

To test if the loss of TBC1D24 function in TBC1D24^{G501R} mutants is the result of a loss of TLDc function we created *sky* mutant flies that express only the TBC domain (TBC1D24$^{\Delta TLDc}$). Interestingly, these animals did not show a defect in FM1–43 distribution (Fig. 4C) and they behave normally (not shown). Collectively, this suggests that under these conditions, the TLDc domain is dispensable for TBC1D24 function and that the TBC1D24^{G501R} mutation exerts a negative effect on the function of the TBC domain.

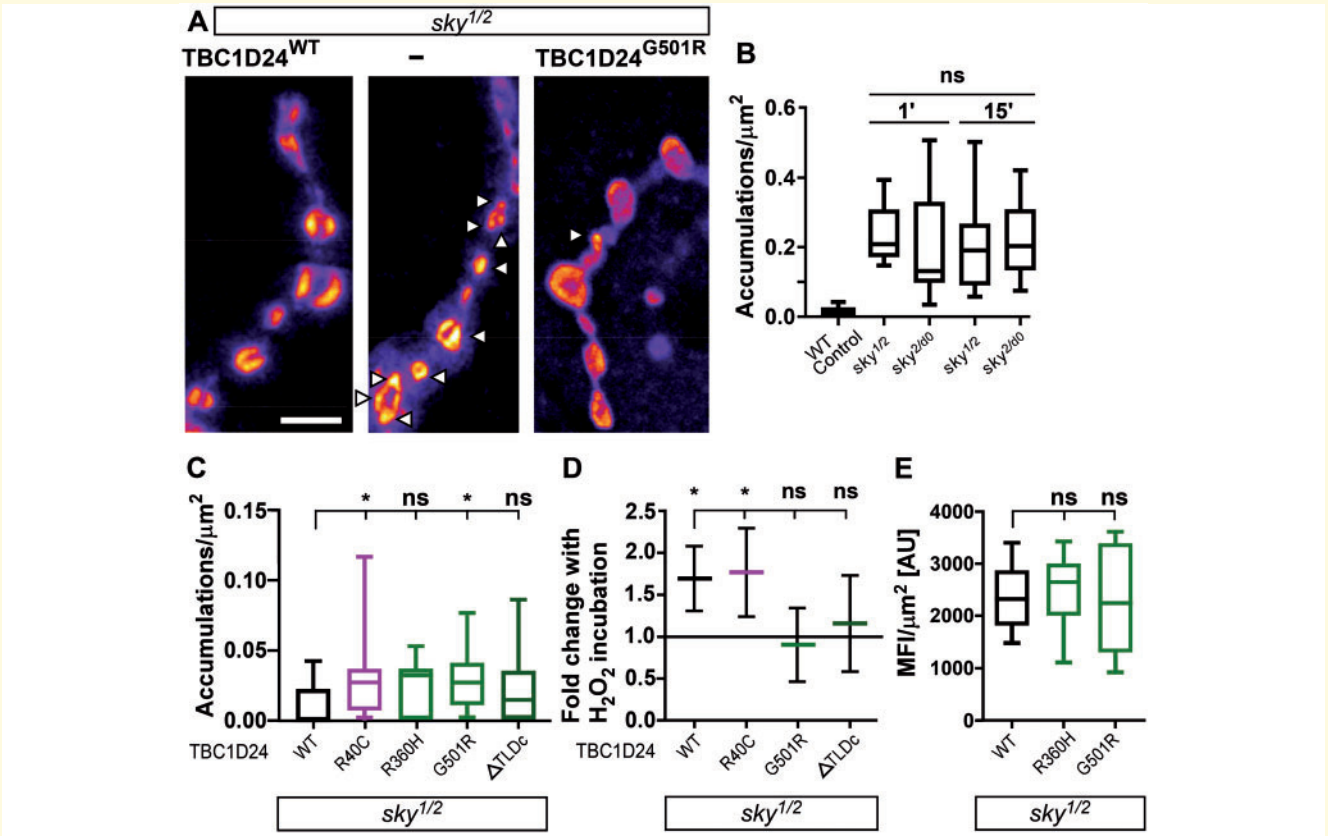

Figure 4 FM1–43. The TBC1D24^{G501R} mutation or oxidative stress increase endocytic vesicle cycling, indicated by accumulations of FM1–43 dye inside the NMJ. (**A** and **B**) The density of endocytic vesicle accumulations in sky$^{1/2}$ or in sky$^{2/d0}$ mutants without overexpression of human TBC1D24 protein is very high even compared to a patient mutation background. These mutants produce high accumulation densities (white arrows) when stimulated immediately or extended incubation in ringer solution. Scale bar = 5 µm. One-way ANOVA: ns = not significant $P = 0.8382$. $n = 4$–5 animals. (**C**) These accumulations occur significantly less often in controls expressing TBC1D24^{WT}. Stimulated TBC1D24^{G501R} NMJ harbour an average of 0.03 puncta/µm^2 compared to a density of ~0.01 puncta/µm^2 in TBC1D24^{WT} NMJ. (**D**) Oxidative stress at the NMJ increases the FM1–43 accumulation density in stimulated boutons of wild-type and TBC domain mutant animals. The R40C mutation in another domain, the TBC domain, results in accumulation numbers comparable to those in TBC1D24^{G501R} in absence of oxidative stress. ROS induced via application of 50 mM H_2O_2 increased the density of endocytosed accumulations in TBC1D24^{WT} and TBC domain mutation TBC1D24^{R40C} 1.6-fold, whereas in the TLDc mutation TBC1D24^{G501R} accumulation density was unchanged by ROS, indicating that the TLDc domain mutation makes TBC1D24 insensitive to oxidative stress. Removal of the entire TLDc domain had no effect on accumulation density, either. One-way ANOVA Kruskal-Wallis test for HL-3-treated TBC1D24^{WT} versus TBC1D24^{R40C}, TBC1D24^{R360H}, TBC1D24^{G501R}, TBC1D24$^{\Delta TLDc}$: *$P = 0.0111$, ns = not significant $P = 0.1158$, *$P = 0.0015$, ns = not significant $P = 0.7339$. Two-way ANOVA: $F(3,130) = 3.05$, *$P = 0.0312$. Holm-Sidak's multiple comparison test for HL-3 versus H_2O_2: TBC1D24^{WT} *$P = 0.0293$, TBC1D24^{R40C} *$P = 0.0155$, TBC1D24^{G501R} ns = not significant $P = 0.9526$, TBC1D24$^{\Delta TLDc}$ ns = not significant $P = 0.9974$. (**E**) Endocytic vesicle uptake rates are unchanged by TLDc mutations. FM1–43 uptake measured as MFI of dye retention in synaptic boutons showed comparable uptake rates for mutant and wild-type TBC1D24 variants. Dunnett's test, TBC1D24^{WT} versus TBC1D24^{R360H}: ns = not significant $P = 0.9682$, versus TBC1D24^{G501R}: ns = not significant $P = 0.8347$. $n = 3$–9 animals.

Synaptic trafficking defects in TBC1D24^{G501R} mutants are caused by ROS

The TLDc domain of TBC1D24 has been implicated in sensing and/or conferring protection to ROS (Finelli *et al.*, 2016). Therefore, we assessed if ROS affects Sky localization and Sky-dependent synaptic vesicle trafficking. First, we exposed synapses that express wild-type and mutant GFP-tagged TBC1D24 to 50 mM H_2O_2 for 15 min but did not observe an effect of ROS on Sky protein abundance or localization (Fig. 2 and Supplementary Table 7).

Next, we determined the effect on FM1–43 labelling following a 15-min H_2O_2 exposure. While untreated control synapses (*sky* mutants that express TBC1D24^{WT}) show very few accumulations of FM1–43, H_2O_2 treatment causes a 1.5-fold increase in the number of FM1–43 accumulations (Fig. 4D). This indicates that ROS acutely affects coordinated vesicle trafficking, consistent with previous studies (Wang and Floor, 1998; Afuwape *et al.*, 2017). Next, we tested the effect of pathogenic mutations. The number of FM1–43-labelled accumulations in H_2O_2-treated *sky* mutants with a mutation in the TBC domain (TBC1D24^{R40C}) was also increased 1.5-fold (Fig. 4D). In contrast, we found that the number of FM1–43 accumulations is neither increased in H_2O_2-treated *sky* mutants that express TBC1D24^{G501R} nor in *sky* mutants that express TBC1D24$^{\Delta TLDc}$; in the latter case, the number of FM1–43 accumulations remains close to zero (Fig. 4D). These results suggest that the vesicle trafficking defect induced by H_2O_2 requires a functional TLDc domain and that TBC1D24^{G501R} mutant affects this role of the TLDc domain.

We investigated the defects in synaptic vesicle trafficking by TEM of synaptic boutons further (Fig. 5A–E). Notably, the total area of large cisternae with a minimum diameter of 80 nm is increased in *sky* mutant boutons that express TBC1D24^{G501R}. This is consistent with previous observations in *sky* loss of function mutants that show an increased number of large cisternae, but here too the phenotype was much stronger (Uytterhoeven *et al.*, 2011; Fischer *et al.*, 2016). This result parallels the increased number of FM1–43 accumulations we observed in animals expressing TBC1D24^{G501R} (Fig. 5A, red arrows). Consistent with functional imaging results, TBC1D24^{R360H} showed only a trend towards an increase in large vesicle surface compared to controls (Supplementary Fig. 3).

We also treated synapses with H_2O_2 before TEM, resulting in increased cisternae in control synapses; however, the number of cisternae in H_2O_2-treated *sky* mutants that express TBC1D24^{G501R} did not change significantly, in line with the FM1–43 phenotype (Fig. 5B and C). Examination of ultrastructural features are comparable between control synapses (*sky* mutants that express TBC1D24^{WT}) and *sky* mutants that express TBC1D24^{G501R}, including the number of active zones and mitochondria (Fig. 5D and E). These data further confirm that ROS-induced vesicle trafficking defects require a functional Sky TLDc domain. Our data are consistent with a model in which pathogenic TLDc domain mutants impair ROS-sensing and protective function of TBC1D24.

Antioxidants rescue defects induced by TLDc mutations

There are two possibilities that might explain our results: (i) the TLDc mutation TBC1D24^{G501R} impairs TLDc function with a consequent TBC-dependent block of vesicle trafficking under control of TBC1D24; and (ii) the mutation causes hypersensitivity to ROS with endogenous ROS levels being high enough to inactivate the mutant TLDc domain, again inhibiting TBC1D24-dependent vesicle trafficking. To distinguish between these possibilities, we treated *sky* mutants that express TBC1D24^{G501R} with *N*-acetylcysteine amide (AD4) or with α-tocopherol (vitamin E). Treatment with AD4 caused a significant rescue of the vesicle trafficking defects as gauged by FM1–43 (Fig. 6A and B). In addition, AD4 also significantly rescued the activity-dependent movement phenotype we observed in *sky* mutants that express TBC1D24^{G501R} (Fig. 6C). α-Tocopherol showed a trend towards rescue in both assays but was not as effective (Fig. 6B and C). It should be noted that neither AD4 nor α-tocopherol increase the activity of TBC1D24^{WT} controls. Feeding with AD4 reduced seizure rates in TBC domain mutant flies as indicated by increased activity scores (Fig. 6D). These results are consistent with a model where the pathogenic mutations that destabilize or affect the conformation of the TLDc domain of TBC1D24, including TBC1D24^{G501R}, cause hypersensitivity to ROS.

Discussion

A 20-year-long follow-up of the original RE-EID family we described in 1998 showed that while epilepsy subsided, with patients experiencing 15 to 22 years seizure freedom, EID attacks persisted in two of the patients. Through sequencing we identified these three patients as the first carriers of compound heterozygous missense mutations within the TLDc domain of TBC1D24, the R360H and G501R mutations, and studied the role of this domain *in vivo*. Furthermore, we identified three additional sporadic patients with a remarkably similar RE-EID phenotype, all carrying a missense mutation in the TLDc domain, the A500V in two and the G511R in the third. Therefore, all six patients reported here carried a missense mutation causing an amino acid substitution in the TLDc domain, between residues 500 and 511, further highlighting the role of this region of the TBCD124 protein in relation to the RE-EID phenotype. In all patients, epilepsy and EID had a maximum of expression in infancy or early childhood. While epilepsy was self-limited or had a relatively benign

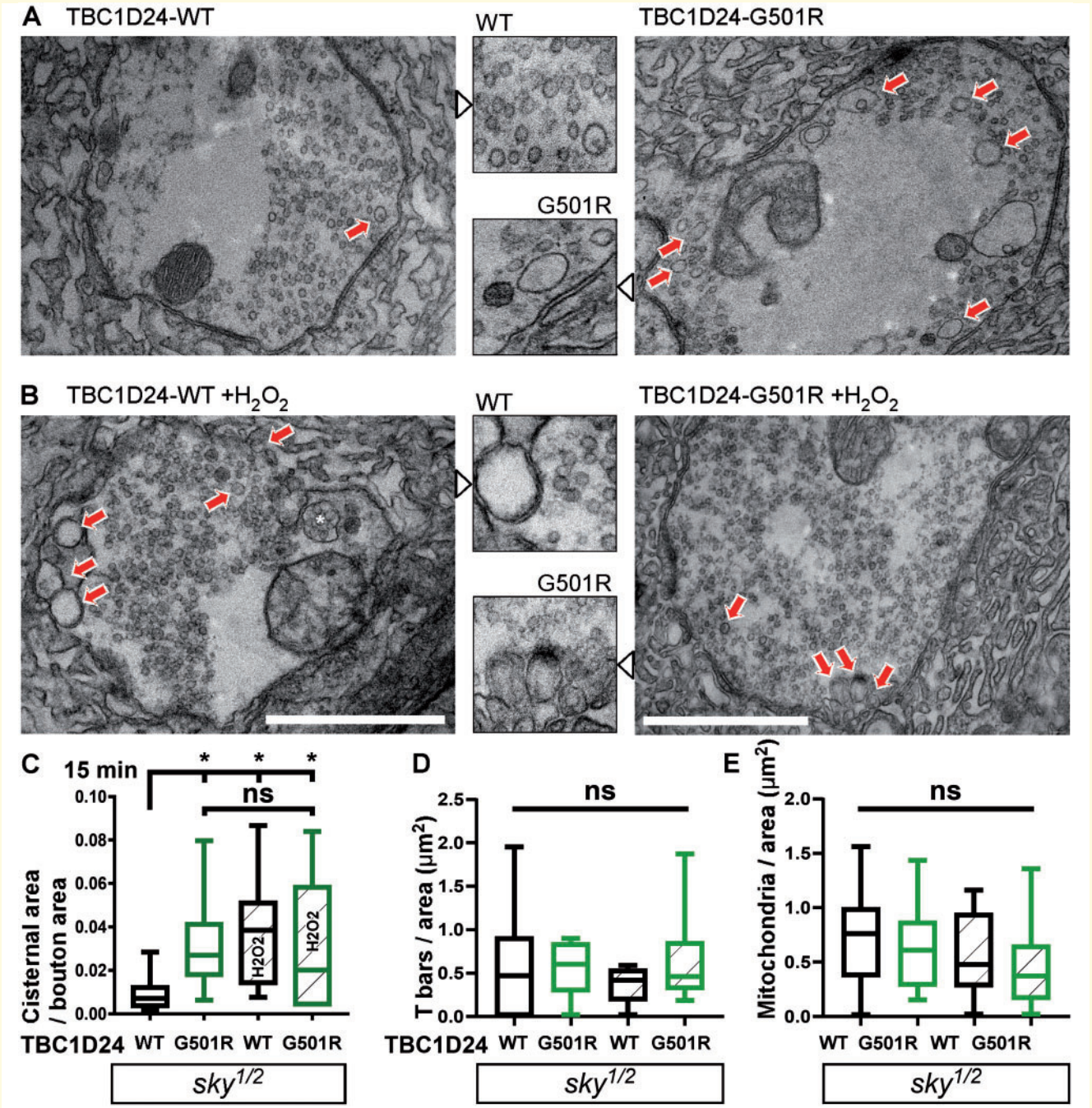

Figure 5 TEM. TEM of stimulated synaptic boutons treated with control buffer or peroxide. (*A*) TBC1D24^{G501R} overexpression on *sky*$^{1/2}$ deficiency background results in high levels of synaptic vesicles > 80 nm. Red arrows point at enlarged synaptic vesicles. Following H_2O_2 treatment delivering oxidative stress to the synapse, stimulated boutons contain a larger fraction of synaptic vesicles in TBC1D24^{WT} compared to the non-treated condition. (**B**) In contrast, TLDc domain mutant TBC1D24^{G501R} animals show no significant peroxide-induced change in large synaptic vesicle areas, while a strong increase is detected in TBC1D24^{WT} following peroxide treatment. Scale bar = 1 µm. (**C**) Quantification of large synaptic vesicle density in peroxide-treated versus non-treated condition. One-way ANOVA, Dunnett's test (cisternal/bouton area): TBC1D24^{WT} versus TBC1D24^{G501R}, TBC1D24^{WT} + H_2O_2, TBC1D24^{G501R} + H_2O_2: **P* = 0.0441, **P* = 0.0124, **P* = 0.0284. Two-way ANOVA, $F(1,40) = 4.306$, **P* = 0.0445. Sidak's test for HL-3 versus H_2O_2: TBC1D24^{WT} ***P* = 0.0090, TBC1D24^{G501R} ns = not significant *P* = 0.9995. (**D**) NMJ synaptic vesicle release sites and (**E**) mitochondria density are unchanged by the G501R and R40C (not shown) mutation at presynaptic terminals. Dunnett's test (T bar): TBC1D24^{WT} versus TBC1D24^{G501R} ns = not significant *P* = 0.8691, versus TBC1D24^{R40C} ns = not significant *P* = 0.4534. Kruskal-Wallis test for TBC1D24^{WT} and TBC1D24^{G501R}, all conditions: ns = not significant *P* = 0.4991. Dunnett's test (mitochondria): TBC1D24^{WT} versus TBC1D24^{G501R} ns = not significant *P* = 0.4202, versus TBC1D24^{R40C} ns = not significant *P* = 0.7951. One-way ANOVA for TBC1D24^{WT} and TBC1D24^{G501R}, all conditions: ns = not significant *P* = 0.2502.

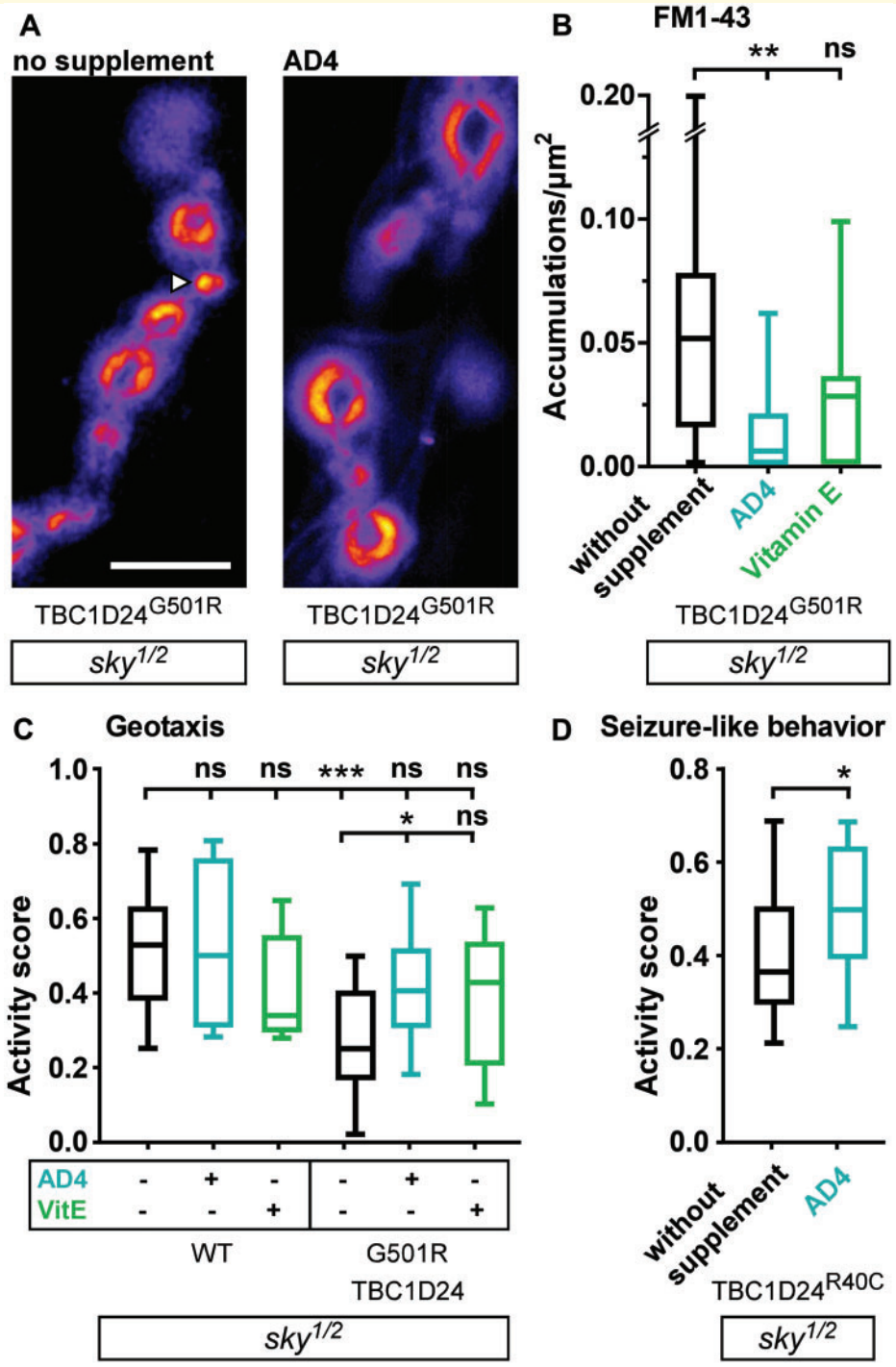

Figure 6 ROS protection rescues TBC1D24^{G501R} phenotype. (**A** and **B**) ROS scavenger efficiently rescued endosomal trafficking defects, indicated by a significant decrease in FM1–43 dye accumulation density in stimulated boutons. Animals were fed with antioxidant *N*-acetylcysteine amide (AD4) or with α-tocopherol (vitamin E) and incubated in physiological HL-3 ringer solution. Compared to animals raised on the same food without supplements, FM1–43 the density of accumulations (white arrow) was significantly lower in the AD4-treated condition. Scale bar = 5 µm. One-way ANOVA: FM1–43, Dunnett's test: TBC1D24^{G501R} (without supplement) versus TBC1D24^{G501R} (AD4): $^{**}P = 0.0065$, TBC1D24^{G501R} (without supplement) versus TBC1D24^{G501R} (VitE): ns = not significant $P = 0.1107$. $n = 5–6$ animals. (**C**) Negative geotaxis performance was significantly higher in AD4-treated TBC1D24^{G501R} animals compared to wild-type controls. Dunnett's test: TBC1D24^{WT}(without supplement) versus TBC1D24^{WT}(AD4) ns = not significant $P = 0.9998$, versus TBC1D24^{WT}(VitE) ns = not significant $P = 0.3751$, versus TBC1D24^{G501R} (without supplement) $^{***}P = 0.0004$, versus TBC1D24^{G501R}(AD4) ns = not significant $P = 0.3457$, versus TBC1D24^{G501R}(VitE) ns = not significant $P = 0.3751$; TBC1D24^{G501R} (without treatment) versus TBC1D24^{G501R} (AD4) $^{*}P = 0.0227$, versus TBC1D24^{G501R}(VitE) ns = not significant $P = 0.3135$. $n = 100–130$ animals. VitE = vitamin E. (**D**) Seizure-like behaviours in the TBC domain mutant TBC1D24^{R40C} are significantly rescued by treatment with antioxidant AD4. Unpaired *t*-test: TBC1D24^{R40C} versus TBC1D24^{R40C}(AD4) $^{*}P = 0.0322$. $n = 70$ animals.

course, with subsequent attenuation, EID was a more prominent and, in some of the patients, longer lasting manifestation.

ROS affects synaptic function (Wang and Floor, 1998; Kaneai *et al.*, 2012) and we show here that the TLDc domain of TBC1D24 can function as a ROS sensor that regulates synaptic vesicle trafficking by controlling TBC1D24 function. Based on the solved crystal structure of the TLDc domain and on functional data, we propose that the RE-EID-associated mutations in the TLDc domain impact on protein domain stability or on the local protein conformation, hence rendering the protein hypersensitive to physiological levels of ROS. We also show that treating animals carrying the RE-EID mutations with antioxidant compounds rescues both clinical (the movement dysfunction) and cellular phenotypes (the synaptic vesicle trafficking defect). Taken together, our work suggests an important role for ROS-load in TBC1D24 pathology.

Several proteins contain TLDc domains, where *in vitro* experiments have suggested a function in oxidative stress protection (Finelli and Oliver, 2017; Finelli *et al.*, 2016, 2019). How the TLDc domain senses ROS is not known, but the stability or conformation of the domain seems to be important, because the targeted mutations in the evolutionarily conserved amino acids involved in ROS protection, as well as the pathogenic mutations we studied here, are predicted to either destabilize the domain or cause changes in the conformation of certain loop regions. We surmise that when the TLDc domain is destabilized or when its structural conformation is locally perturbed, ROS access to critical regions of the protein domain is facilitated. In this scenario, destabilizing mutations would be more sensitive to ROS to the degree that endogenous ROS levels may already suffice to affect the TLDc domain. This is consistent with our observations because (i) the effects of the TBC1D24^{G501R} mutant are rescued by antioxidants; (ii) the vesicle trafficking defect of TBC1D24^{G501R} is not worsened when synapses are exposed to additional ROS; (iii) defects caused by mutations in the TBC domain that are not expected to destabilize the TLDc domain are significantly exacerbated in the presence of ROS; and (iv) TBC1D24 mutants that lack the TLDc domain do not show vesicle trafficking defects under endogenous conditions or under high ROS conditions. Although rescue by antioxidants may intuitively suggest forthcoming clinical applications, an appropriate trial design would be required to explore if our experimental findings have translational consequences in human pathology. At this stage, we cannot draw any conclusion from the seemingly unsuccessful administration of ubidecarenone in one of our adult patients, due to the brief treatment period and the uncontrolled nature of the observation.

Skywalker/TBC1D24 regulates synaptic vesicle trafficking, a function encompassed by the TBC domain that interacts with small Rab-GTPases (Frasa *et al.*, 2012). Indeed, pathogenic mutations located in the TBC domain cause synaptic vesicle trafficking defects in fruit flies (Fischer *et al.*, 2016). We show here that mutations in the TLDc domain of human TBC1D24 also result in synaptic vesicle trafficking defects in fruit flies, suggesting a functional interaction between TLDc and TBC domains. Our attempts to generate full-length TBC1D24/Skywalker crystals have not yet been successful. Hence, we do not know the nature of possible physical interactions between TLDc and TBC, but several lines of evidence are pointing to the potential cooperation between the two domains. Indeed, mutations in the TLDc domain of another protein, Oxr1, result in severe loss-of-function of the full-length isoform suggesting that mutating the TLDc domain was sufficient to affect the rest of the protein (Finelli and Oliver, 2017).

Our work suggests a model where part of the function of a major regulator of synaptic vesicle trafficking, TBC1D24/Sky, is regulated by ROS levels. High ROS load causes damage to biomolecules, temporary neuronal hyperactivity and neuronal loss (Wang and Floor, 1998; Aguiar *et al.*, 2012; Kaneai *et al.*, 2012), but, as we suggest here, it also appears to target the TLDc domain of TBC1D24/Sky, causing the entire protein to become less active. Our previous work shows that inactive TBC1D24/Sky results in increased trafficking of vesicles to endosomes where dysfunctional proteins are sorted for degradation (Uytterhoeven *et al.*, 2011; Fernandes *et al.*, 2014; Sheehan *et al.*, 2016). We assume that the TLDc domain's role as a potential ROS sensor in TBC1D24/Sky may be particularly relevant at synapses. These compartments are often maintained far from the cell body and need to cope with dysfunctional proteins and lipids autonomously from the neuronal cell body (Vijayan and Verstreken, 2017). We propose that the TLDc domain senses higher synaptic ROS levels and this causes inactivation of the entire TBC1D24, thus promoting vesicle protein trafficking to, and sorting at, endosomes and finally maintaining synaptic protein homeostasis. This also explains why TBC1D24$^{\Delta TLDc}$ remains inert in the presence of ROS.

Mutations in *TBC1D24* cause a spectrum of phenotypes, with epilepsy being a major manifestation, yet varying in type and severity. Our observation adds another class of phenotypes that encompass an epilepsy-EID syndrome and is caused by compound heterozygous missense mutations with involvement of the TLDc domain, particularly between amino acid residues 500 to 511. In patients with mutations limited to the TBC domain, EID has not been reported and epilepsy is often severe and not self-limited.

In most sporadic patients and dominant families with EID, causative mutations affect the *PRRT2* gene and benign infantile seizures are also observed (Marini *et al.*, 2012). PRRT2 (OMIM*614386) is a proline-rich transmembrane protein. Although its function remains relatively unknown, yeast two-hybrid studies suggest that PRRT2 interacts with synaptosomal-associated protein 25 kD (SNAP25) (Stelzl *et al.*, 2005). PRRT2 knockout primary cultures and acute hippocampal slices show slowdown of the kinetics of exocytosis in excitatory neurons with weakened spontaneous and evoked synaptic transmission,

while inhibitory neurons show strengthening of basal synaptic transmission and faster depression (Valente *et al.*, 2018).

EID, often associated with epilepsy, is also observed in patients with mutations of *SLC2A1* (or *GLUT1*) (OMIM*138140), a gene coding for the glucose-transporter-type-1, which assures the energy-independent, facilitative transport of glucose into the brain (Thorens and Mueckler, 2010). A similar phenotype is rarely observed also in carriers of mutations causing early-onset parkinsonism (such as parkin, *PRKN*, OMIM*602544) or DOPA-responsive dystonia (such as *GCH1*, OMIM*602544) (Silveira-Moriyama *et al.*, 2018). The clinical context of the latter conditions, however, does not require differential diagnosis with the *TBC1D24* phenotype we are describing.

Sky mutant fruit flies that express human pathogenic TLDc mutations show motor defects but no apparent seizure-like behaviour, consistent with the idea that 'TLDc only' mutations may be at one extreme of the TBC1D24 phenotypic spectrum. However, epilepsy was mild and only expressed in a narrow age range in RE-EID patients and mild seizure-like attacks in flies might have escaped recognition. Descriptions of additional patients carrying 'TLDc only' mutations will clarify this notion. We observed vesicle trafficking defects both in flies expressing TBC mutations and in those expressing TLDc mutations; the difference between them being that synapses of flies expressing 'TLDc only' mutations lost the ROS sensitivity to regulate TBC1D24-dependent vesicle trafficking, which might underpin the observed phenotype differences.

We describe a new genetic cause of EID co-occurring with mild age-related epilepsy, likewise observed in patients with *PRRT2* mutations. We previously reported the effect of TBC mutations on the molecular structure of the TBC domain, where mutations in a unique positively charged pocket that binds the lipid $PI(4,5)P_2$, or other 5-phosphorylated phospholipids, lead to a decreased affinity for these lipids (Fischer *et al.*, 2016). This is resolved by genetically enhancing $PI(4,5)P_2$ levels, which rescues the clinical defects of the mutant animal model (Fischer *et al.*, 2016). Now we add another tile to a possible therapeutic strategy for TBC1D24-associated diseases, namely combining agents that increase synaptic $PI(4,5)P_2$ levels, targeting TBC dysfunction, together with antioxidants, which target TLDc mutant hypersensitivity to ROS.

Acknowledgements

We thank Willem Van den Bergh for *Drosophila* embryonic injection of transgenic constructs, Ann Geens and Sebastian Munck for statistical analysis support, as well as Sabine Kuenen and Ulrike Pech for valuable feedback on seizure characterization.

We would like to thank the staff at the beamlines Proxima 2 of Soleil (France) for assistance during data collection.

Funding

This work was supported by the Fonds voor Wetenschappelijk Onderzoek, an ERC consolidator grant, the Hercules Foundation, the Vlaamse Parkinson Liga, a Methusalem grant of the Flemish government, VIB, a Strategic Research Program Financing of the VUB, BioStruct-X, by the European Commission Seventh Framework Programme (DESIRE project). PV is a member of the FENS Kavli Network of Excellence. I.M. was supported by the American Academy of Neurology Institute and the American Brain Foundation through a Clinical Research Training Fellowship.

Competing interests

The authors report no competing interests.

Supplementary material

Supplementary material is available at *Brain* online.

References

Afuwape OAT, Wasser CR, Schikorski T, Kavalali ET. Synaptic vesicle pool-specific modification of neurotransmitter release by intravesicular free radical generation. J Physiol 2017; 595: 1223–38.

Aguiar CCT, Almeida AB, Araújo PVP, de Abreu RNDC, Chaves EMC, do Vale OC, et al. Oxidative stress and epilepsy: literature review. Oxid Med Cell Longev 2012; 2012: 795259.

Appavu B, Guido-Estrada N, Lindstrom K, Grebe T, Kerrigan JF, Troester M. Electroclinical phenotypes and outcomes in TBC1D24-related epilepsy. Epileptic Disord 2016; 18: 324–28.

Atli E, Gurkan H, Ulusal S, Karal Y, Atli EI, Tozkir H. Identification of a novel homozygous TBC1D24 mutation in a Turkish family with DOORS syndrome. Clin Dysmorphol 2018; 27: 1–3.

Balestrini S, Milh M, Castiglioni C, Lüthy K, Finelli MJ, Verstreken P, et al. TBC1D24 genotype-phenotype correlation: epilepsies and other neurologic features. Neurology 2016; 87: 77–85.

Benzer S. Behavioral mutants of Drosophila isolated by countercurrent distribution. Proc Natl Acad Sci USA. 1967; 58: 1112–9.

Blaise M, Alsarraf HMAB, Wong JEMM, Midtgaard SR, Laroche F, Schack L, et al. Crystal structure of the TLDc domain of oxidation resistance protein 2 from zebrafish. Proteins 2012; 80: 1694–8.

Chen D, Wilkinson CRM, Watt S, Penkett CJ, Toone WM, Jones N, et al. High-resolution crystal structure and in vivo function of a kinesin-2 homologue in giardia intestinalis. Mol Biol Cell 2007; 19: 308–17.

Dehouck Y, Grosfils A, Folch B, Gilis D, Bogaerts P, Rooman M. Fast and accurate predictions of protein stability changes upon mutations using statistical potentials and neural networks: PoPMuSiC-2.0. Bioinformatics 2009; 25: 2537–43.

Driver C, Georgeou A. Variable effects of vitamin E on drosophila longevity. Biogerontology 2003; 4: 91–5.

Emsley P, Lohkamp B, Scott WG, Cowtan K. Features and development of coot. Acta Crystallogr D Struct Biol 2010; 66: 486–501.

Estes PS, Roos J, van der Bliek A, Kelly RB, Krishnan KS, Ramaswami M. Traffic of dynamin within individual Drosophila synaptic boutons relative to compartment-specific markers. J Neurosci 1996; 16: 5443–56.

Falace A, Buhler E, Fadda M, Watrin F, Lippiello P, Pallesi-Pocachard E, et al. TBC1D24 regulates neuronal migration and maturation through modulation of the ARF6-dependent pathway. Proc Natl Acad Sci U S A 2014; 111: 2337–42.

Falace A, Filipello F, La Padula V, Vanni N, Madia F, De Pietri Tonelli D, et al. TBC1D24, an ARF6-interacting protein, is mutated in familial infantile myoclonic epilepsy. Am J Hum Genet 2010; 87: 365–70.

Fernandes AC, Uytterhoeven V, Kuenen S, Wang Y-C, Slabbaert JR, Swerts J, et al. Reduced synaptic vesicle protein degradation at lysosomes curbs TBC1D24/sky-induced neurodegeneration. J Cell Biol 2014; 207: 453–62.

Finelli MJ, Aprile D, Castroflorio E, Jeans A, Moschetta M, Chessum L, et al. The epilepsy-associated protein TBC1D24 is required for normal development, survival and vesicle trafficking in mammalian neurons. Hum Mol Genet 2019; 28: 584–97.

Finelli MJ, Oliver PL. TLDc proteins: new players in the oxidative stress response and neurological disease. Mamm Genome 2017; 28: 395–406.

Finelli MJ, Sanchez-Pulido L, Liu KX, Davies KE, Oliver PL. The evolutionarily conserved Tre2/Bub2/Cdc16 (TBC), lysin motif (LysM), domain catalytic (TLDc) domain is neuroprotective against oxidative stress. J Biol Chem 2016; 291: 2751–63.

Fischer B, Lüthy K, Paesmans J, De Koninck C, Maes I, Swerts J, et al. Skywalker-TBC1D24 has a lipid-binding pocket mutated in epilepsy and required for synaptic function. Nat Struct Mol Biol 2016; 23: 965–73.

Frasa MAM, Koessmeier KT, Ahmadian MR, Braga VMM. Illuminating the functional and structural repertoire of human TBC/RABGAPs. Nat Rev Mol Cell Biol 2012; 13: 67–73.

Guerrini R, Bonanni P, Nardocci N, Parmeggiani L, Piccirilli M, De Fusco M, et al. Autosomal recessive rolandic epilepsy with paroxysmal exercise-induced dystonia and writer's cramp: delineation of the syndrome and gene mapping to chromosome 16p12–11.2. Ann Neurol 1999; 45: 344–52.

Ioannidis NM, Rothstein JH, Pejaver V, Middha S, McDonnell SK, Baheti S, et al. REVEL: an ensemble method for predicting the pathogenicity of rare missense variants. Am J Hum Genet 2016; 99: 877–85.

Ionita-Laza I, McCallum K, Xu B, Buxbaum JD. A spectral approach integrating functional genomic annotations for coding and noncoding variants. Nat Genet 2016; 48: 214–20.

Jagadeesh KA, Wenger AM, Berger MJ, Guturu H, Stenson PD, Cooper DN, et al. M-CAP eliminates a majority of variants of uncertain significance in clinical exomes at high sensitivity. Nat Genet 2016; 48: 1581–6.

Jung W, Liu C, Yu Y, Chang Y, Lien W, Chao H, et al. Lipophagy prevents activity-dependent neurodegeneration due to dihydroceramide accumulation in vivo. EMBO Rep 2017; 18: 1150–65.

Kabsch W. XDS. Acta Crystallogr D Struct Biol 2010; 66: 125–32.

Kaneai N, Arai M, Takatsu H, Fukui K, Urano S. Vitamin e inhibits oxidative stress-induced denaturation of nerve terminal proteins involved in neurotransmission. J Alzheimers Dis 2012; 28: 183–9.

Kwak SH, Chae JHJ, Choi S, Kim MJ, Choi M, Chae JHJ, et al. Findings of a 1303 Korean whole-exome sequencing study. Exp Mol Med 2017; 49: e356.

Li J, Liu R, Feng H, Zhang J, Wang D, Wang Y, et al. Novel TBC1D24 mutations in a case of nonconvulsive status epilepticus. Front Neurol 2018; 9: 623.

Liu X, Wu C, Li C, Boerwinkle E. dbNSFP v3.0: a one-stop database of functional predictions and annotations for human nonsynonymous and splice-site SNVs. Hum Mutat 2016; 37: 235–41.

Marini C, Conti V, Mei D, Battaglia D, Lettori D, Losito E, et al. PRRT2 mutations in familial infantile seizures, paroxysmal dyskinesia, and hemiplegic migraine. Neurology 2012; 79: 2109–14.

McCoy AJ, Grosse-Kunstleve RW, Adams PD, Winn MD, Storoni LC, Read RJ. Phaser crystallographic software. J Appl Crystallogr 2007; 40: 658–74.

Milh M, Falace A, Villeneuve N, Vanni N, Cacciagli P, Assereto S, et al. Novel compound heterozygous mutations in TBC1D24 cause familial malignant migrating partial seizures of infancy. Hum Mutat 2013; 34: 869–72.

Muona M, Berkovic SF, Dibbens LM, Oliver KL, Maljevic S, Bayly MA, et al. A recurrent de novo mutation in KCNC1 causes progressive myoclonus epilepsy. Nat Genet 2015; 47: 39–46.

Ngoh A, Bras J, Guerreiro R, McTague A, Ng J, Meyer E, et al. TBC1D24 Mutations in a sibship with multifocal polymyoclonus. Tremor Other Hyperkinet Mov 2017; 7: 452.

Ragona F, Castellotti B, Salis B, Magri S, DiFrancesco JC, Nardocci N, et al. Alternating hemiplegia and epilepsia partialis continua: a new phenotype for a novel compound TBC1D24 mutation. Seizure 2017; 47: 71–3.

Ramaswami M, Krishnan KS, Kelly RB. Intermediates in synaptic vesicle recycling revealed by optical imaging of drosophila neuromuscular junctions. Neuron 1994; 13: 363–75.

Sawin-McCormack EP, Sokolowski MB, Campos AR. Characterization and genetic analysis of Drosophila melanogaster photobehavior during larval development. J Neurogenet 1995; 10: 119–35.

Sheehan P, Waites CL. Coordination of synaptic vesicle trafficking and turnover by the Rab35 signaling network. Small GTPases 2019; 10: 54–63.

Sheehan P, Zhu M, Beskow A, Vollmer C, Waites CL. Activity-dependent degradation of synaptic vesicle proteins requires Rab35 and the ESCRT pathway. J Neurosci 2016; 36: 8668–86.

Silveira-Moriyama L, Kovac S, Kurian MA, Houlden H, Lees AJ, Walker MC, et al. Phenotypes, genotypes, and the management of paroxysmal movement disorders. Dev Med Child Neurol 2018; 60: 559–65.

Slabbaert JR, Kuenen S, Swerts J, Maes I, Uytterhoeven V, Kasprowicz J, et al. Shawn, the drosophila homolog of SLC25A39/40, is a mitochondrial carrier that promotes neuronal survival. J Neurosci 2016; 36: 1914–29.

Stelzl U, Worm U, Lalowski M, Haenig C, Brembeck FH, Goehler H, et al. A human protein-protein interaction network: a resource for annotating the proteome. Cell 2005; 122: 957–68.

Thorens B, Mueckler M. Glucose transporters in the 21st century. Am J Physiol Endocrinol Metab 2010; 298: E141–5.

Tona R, Chen W, Nakano Y, Reyes LD, Petralia RS, Wang YX, et al. The phenotypic landscape of a Tbc1d24 mutant mouse includes convulsive seizures resembling human early infantile epileptic encephalopathy. Hum Mol Genet 2019; 28: 1530–47.

Uytterhoeven V, Kuenen S, Kasprowicz J, Miskiewicz K, Verstreken P. Loss of skywalker reveals synaptic endosomes as sorting stations for synaptic vesicle proteins. Cell 2011; 145: 117–32.

Valente P, Romei A, Fadda M, Sterlini B, Lonardoni D, Forte N, et al. Constitutive inactivation of the PRRT2 gene alters short-term synaptic plasticity and promotes network hyperexcitability in hippocampal neurons. Cereb Cortex 2018; 29: 2010–33.

Vijayan V, Verstreken P. Autophagy in the presynaptic compartment in health and disease. J Cell Biol 2017; 216: 1895–906.

Wang Y, Floor E. Hydrogen peroxide inhibits the vacuolar H+-ATPase in brain synaptic vesicles at micromolar concentrations. J Neurochem 1998; 70: 646–52.

Worth CL, Preissner R, Blundell TL. SDM: a server for predicting effects of mutations on protein stability and malfunction. Nucleic Acids Res 2011; 39: W215–22.

Zhou Q, Lin Y, Ye J, Li L, Hu N, Wang D, et al. Homozygous TBC1D24 mutation in a case of epilepsia partialis continua. Front Neurol 2018; 8: 750.